Faraday Discussions
Cite this: DOI: 10.1039/d5fd00169b

PAPER

Co-adsorption of aniline and H_2 over Pd/Al_2O_3: an infrared spectroscopic study

Annelouise M. McCullagh and David Lennon *

Received 15th December 2025, Accepted 21st January 2026
DOI: 10.1039/d5fd00169b

In order to rationalise high aniline selectivity in nitrobenzene hydrogenation over alumina-supported Pd catalysts, the adsorption-complex geometry of aniline during co-adsorption of H_2 and aniline on a 5 wt% Pd/Al_2O_3 catalyst is investigated *via* infrared spectroscopy. With respect to molecular symmetry and the metal-surface selection rule, observation of solely out-of-plane aniline modes at low aniline exposures at 30 °C indicate a parallel orientation of aniline with respect to the Pd surface. The simultaneous emergence of negative hydroxyl features indicate adsorption occurs at the metal/support interface. Increasing exposure reveals additional adsorption of aniline to a range of hydroxyls of the alumina support. The full range of adsorption spectra reveal that the presence of H_2 in the co-feed accelerates aniline adsorption to the catalyst and permits reagent hydrogenation to cyclohexylamine. Temperature-programmed infrared measurements show no change in the adsorption-complex geometry as a function of surface coverage. A previous reaction scheme is modified in which nitrobenzene and aniline adsorption geometry are intrinsically related to the high aniline selectivity reported for Pd/Al_2O_3 catalysts.

1. Introduction

Aniline synthesis catalysis *via* nitrobenzene hydrogenation is an established reaction of some significance.[1–6] Not least as part of the production chain for the manufacture of methylene diphenyl diisocyanate, a key component in polyurethane production.[7] Recent work by the authors has examined the case for the application of Pd/Al_2O_3 as an aniline synthesis catalyst that is able to facilitate highly selective aniline synthesis in nitrobenzene hydrogenation, with over-hydrogenation of aniline identified as the principal route to by-product formation.[2,6,8,9] This over-hydrogenation is a three-step process producing cyclohexylamine (CHA) from hydrogenation of the aniline aromatic ring, *N*-cyclohexylaniline (CHAN) from coupling of aniline and CHA, and finally dicyclohexylamine (DICHA) from hydrogenation of the aromatic moiety of CHAN (Scheme 1).

School of Chemistry, University of Glasgow, Joseph Black Building, Glasgow, G12 8QQ, UK. E-mail: David.Lennon@glasgow.ac.uk; Tel: +44-141-330-4372

Scheme 1 Aniline hydrogenation to cyclohexylamine (CHA), *N*-cyclohexylaniline (CHAN) and dicyclohexylamine (DICHA). Adapted from ref. 6. Copyright – CC BY 4.0.

Aniline comprises an aromatic ring and an amine group, both inherently capable of interacting with metal surfaces, potentially influencing adsorption geometry and catalytic performance. Surface science has proved influential in understanding adsorbate/substrate bonding configurations. For example, Rockey *et al.* examined aniline adsorption on Ag(111) using high-resolution electron energy loss spectroscopy.[10] Two distinct peaks were observed: an out-of-plane ring deformation at 486 cm^{-1} and an out-of-plane C–H bend at 737 cm^{-1}. The absence of in-plane modes indicated parallel adsorption, with spectral deconvolution estimating a tilt angle of 13 $\pm$ 8°, and adsorption was proposed to occur *via* the amino group.

Huang *et al.* explored aniline orientation and hydrogenolysis species on Pt(111) using temperature-programmed reaction and NEXAFS.[11] Analysis of π^* and σ^* resonance intensities relative to the incidence angle revealed that, in the absence of hydrogen, the aromatic ring was tilted with respect to Pt(111), with a maximum tilt of ~31°; π-bonding between the ring and Pt dominated under these conditions. In contrast, hydrogen co-adsorption induced a predominantly parallel orientation, suggesting a stronger interaction involving both π-electrons and the nitrogen lone pair. Thus, hydrogen significantly influences both orientation and binding strength.

Computational studies corroborate these findings. Alsunaidi *et al.* reported parallel adsorption of aniline on Ni(111) during benzene amination, with C–H bonds buckled away from the surface.[12] Binding involved π-interactions at bridging sites and σ-interactions at on-top sites *via* NH_2. Similar configurations were predicted by Tezsevin *et al.* for Ru(0001) and Co(0001),[13] and by Henríquez-Román *et al.* for Cu defect sites, including steps, kinks, and corners.[14]

Regarding aniline adsorption on supported metal catalysts, previous work by the authors used infrared spectroscopy to examine nitrobenzene adsorption on a 5 wt% Pd/Al_2O_3 catalyst and established that nitrobenzene adopts a vertical monodentate adsorption geometry on the Pd crystallites, alongside aniline re-adsorption onto the inactive alumina support through hydrogen bonding with surface hydroxyls.[15] An investigation into structure–activity relationships for Pd/Al_2O_3 catalysts during nitrobenzene hydrogenation identified the concomitant shut-down of aniline over-hydrogenation chemistry with poisoning of the Pd(100) site.[8] Thus, it was postulated that nitrobenzene hydrogenation activity occurs on the dominant Pd(111) facets, whilst aniline hydrogenation is facilitated by the minimised Pd(100) facets. Furthering this, a combined spectroscopic and computational investigation on sole aniline adsorption on Pd/Al_2O_3 confirmed aniline adsorption on the inactive alumina support alongside parallel aniline adsorption at the Pd(100)/support interfacial sites.[16]

Recent reaction testing of aniline hydrogenation over the same Pd/Al_2O_3 catalyst demonstrated low activity in strongly reducing conditions at elevated temperature.[17] Although this outcome qualitatively confirms the low formation of aniline-derived by-products during nitrobenzene hydrogenation over supported Pd catalysts, there remains a need to rationalise these favourable outcomes in terms of adsorbate geometry under actual reaction conditions. Against this background, the present study investigates aniline adsorption geometry over the aforementioned 5 wt% Pd/Al_2O_3 catalyst with a hydrogen co-feed, *i.e.*, during catalytic turnover, to advance understanding of the origins of high aniline selectivity over Pd catalysts under hydrogenation conditions.

2. Experimental

In situ diffuse-reflectance infrared Fourier transform spectroscopy (DRIFTS) measurements were conducted using a Bruker Vertex 70 FT-IR spectrometer equipped with an MCT detector. The catalyst (5 wt% Pd/Al_2O_3; Alfa Aesar: 11713) was used as-received in powder form, with approximately 50 mg placed in a Harrick Praying Mantis reaction chamber fitted with an ATC heater for temperature control.

Catalyst activation was performed *in situ* under a flow of helium (35 mL min^{-1}, BOC, 99.9%) and hydrogen (15 mL min^{-1}, BOC, 99.8%) while heating to 110 °C, held for 30 min. The temperature was then increased to 200 °C for 1 h, with hydrogen flow stopped after 30 min. The sample was cooled to ambient temperature under helium and purged for 18 h to minimize residual hydrogen, which could otherwise promote uncontrolled aniline hydrogenation. A background spectrum was recorded at 28 °C.

Aniline was introduced *via* a bubbler system delivering 54.0 $\mu mol_{(ANL)}$ min^{-1} $g_{(cat)}^{-1}$ in the vapor phase using helium as the carrier gas. Hydrogen was introduced to the cell *via* a mass flow controller (Brooks) delivering 1.37 $mmol_{(H_2)}$-min^{-1} $g_{(cat)}^{-1}$. Spectra (aniline : H_2 = 1 : 25 v/v) were collected at defined intervals during adsorption to quantify aniline uptake. For desorption studies, the catalyst was heated under helium to the target temperature, held for 30 min, then cooled to 28 °C for spectral acquisition. This procedure was repeated for 60, 100, 120, 160, and 200 °C. All spectra were recorded at 30 °C using 520 scans at 4 cm^{-1} resolution and presented as difference spectra (activated-catalyst spectrum subtracted from aniline-dosed spectrum) without additional processing.

3. Results

Key aniline modes for orientational diagnostics were assigned by the authors previously.[16] These are the ν(Ph–NH_2), ν(CC) [$\mathcal{M}_{24}$], ν(CC) [$\mathcal{M}_4$], and $\delta_{oop}(NH_2)$ modes observed at *ca.* 1280, 1500, 1600 and 1620 cm^{-1}, respectively. Table S1 in the SI presents wavenumber assignments.

3.1 Adsorption geometry: function of aniline & H_2 surface coverage

Incremental co-adsorption of aniline (exposures of 0.11–4.86 mmol $g_{(cat)}^{-1}$) and hydrogen (exposures of 2.75–122 mmol $g_{(cat)}^{-1}$) on 5 wt% Pd/Al_2O_3 produced spectra (Fig. 1) that reveal both adsorbed aniline and hydrogenation products.

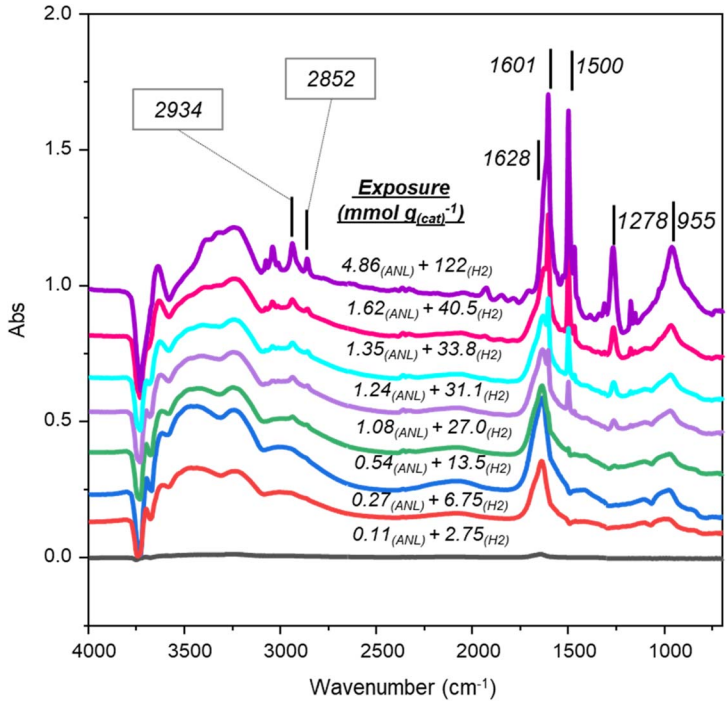

Fig. 1 DRIFTS spectra (4000–700 cm^{-1}) depicting increasing aniline and hydrogen (0.11–4.86 $mmol_{(ANL)}$ $g_{(cat)}{}^{-1}$ and 2.75–122 $mmol_{(H_2)}$ $g_{(cat)}{}^{-1}$) exposure to Pd/Al_2O_3 at 30 °C. The spectra have been offset to facilitate viewing.

At low reagent exposures (≤0.54 $mmol_{(ANL)}$ and 13.5 $mmol_{(H_2)}$) the following features are noted: (i) a broad peak at *ca.* 1640 cm^{-1} assigned to $\delta_{oop}(NH_2)$, (ii) a broad feature from 3500–3000 cm^{-1} that is associated with aniline NH_2 hydrogen bonding to the catalyst, and (iii) negative hydroxyl features at *ca.* 3750–3650 cm^{-1}. The absence of in-plane aniline modes is indicative of a parallel adsorption of aniline at the metal surface. Due to the background subtraction procedure deployed (Section 2), the negative hydroxyl features represent perturbation of alumina surface hydroxyls after aniline adsorption and identifies these hydroxyls as adsorption sites.[16] The coincidence of aniline adsorption parallel to the Pd surface and aniline adsorption at support hydroxyls indicates adsorption at the metal/support interface under this coverage regime.

At maximum exposure, all key aniline modes are evident: in-plane A′ ν(CC) and ν(Ph–NH_2) at 1601 and 1278 cm^{-1}, in-plane A″ ν(CC) at 1500 cm^{-1}, and out-of-plane A′ $\delta_{oop}(NH_2)$ at 1628 cm^{-1}. Collectively, these modes match the spectrum for sole aniline adsorption to the alumina support, as reported previously.[16] However, two additional sharp bands at 2934 and 2852 cm^{-1} are noted, and are assigned to the $\nu_{AS}(CH_2)$ and $\nu_S(CH_2)$ of cyclohexylamine (CHA), confirming partial hydrogenation of aniline in the presence of hydrogen.[18,19]

Peak area analysis (Fig. S1, SI) shows aniline approaching saturation, while CHA bands increase continuously with coverage. This divergence of profiles is indicative of adsorption occurring on distinct sites: (i) aniline adsorption involves

hydroxyl groups and the Pd(100)[8]/support interface, and (ii) CHA on additional sites. The attribution that the aniline metal adsorption sites are Pd(100) facets originates from McCullagh and co-workers' study of solely aniline adsorption on Pd/Al_2O_3.[16] On the basis of relative peak intensities, CHA formation remains minor compared to aniline adsorption; this is consistent with reaction testing outcomes.[17] This mechanistic insight underscores the role of hydrogen in modifying adsorption geometry and promoting transformation pathways on Pd/γ-Al_2O_3. A literature comparison indicates that CHA adopts the equatorial conformer under these conditions, supported by $\nu_{AS}(CH_2)$ at 2934 cm^{-1}.[13]

Fig. 2 presents the hydroxyl-stretch region during co-adsorption of aniline and hydrogen to the catalyst and reproduces trends comparable to those reported for sole aniline adsorption over Pd/Al_2O_3.[16] Specifically, negative features depicted at 3754, 3728 and 3690 cm^{-1} are associated with H-bonded type IIa, type IIb and type III hydroxyl groups, respectively.[20] Thus, during co-adsorption with hydrogen, aniline is partitioned over the same three hydroxyl groups present on the inactive γ-Al_2O_3 support *via* H-bonding.

Some differences in the ν(O–H) band profiles for sole aniline adsorption[16] and aniline/hydrogen co-adsorption are noted. Specifically, the negative feature at *ca.* 3728 cm^{-1}, attributable to type IIb hydroxyl groups,[20] is observable at lower exposures in the co-adsorption measurements and remains prominent at higher exposures. It is therefore assumed that the presence of hydrogen in the co-feed is facilitating H-bonding to the hydroxyl groups of the alumina support.

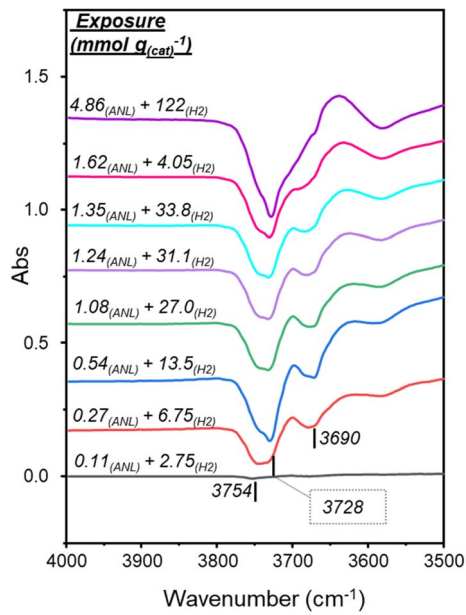

Fig. 2 DRIFTS spectra (4000–3500 cm^{-1}) depicting the hydroxyl group stretching region during increasing aniline and hydrogen (0.11–4.86 $mmol_{(ANL)}$ $g_{(cat)}^{-1}$ and 2.75–122 $mmol_{(H_2)}$ $g_{(cat)}^{-1}$) exposure to Pd/Al_2O_3 at 30 °C. The spectra have been offset to facilitate viewing.

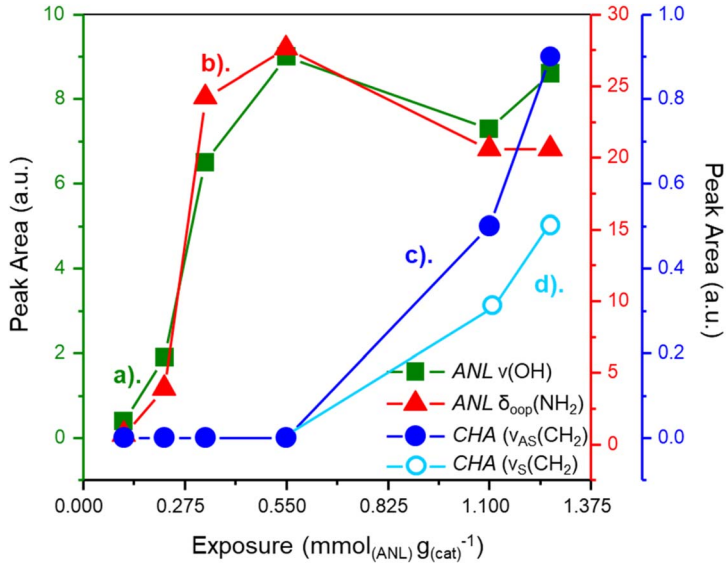

Fig. 3 Plot of peak area for bands corresponding to the (a) H-bonded ν(OH) of Pd/Al_2O_3, (b) the aniline $\delta_{oop}(NH_2)$ mode, and the cyclohexylamine (c) $\nu_{AS}(CH_2)$ and (d) $\nu_S(CH_2)$ modes as a function of increasing aniline and H_2 exposure to 5 wt% Pd/Al_2O_3. Note: the x-axis displays aniline exposure only.

Fig. 3 presents IR peak areas of diagnostic aniline and CHA bands in the lower exposure range ($0.11_{(ANL)} + 2.75_{(H_2)}$ to $1.24_{(ANL)} + 31.1_{(H_2)}$ mmol $g_{(cat)}^{-1}$) For clarity, the negative ν(OH) feature—indicative of H-bonding between Pd/Al_2O_3 hydroxyls and aniline—is plotted as a positive value, so an increase reflects stronger H-bonding. Peak areas for ν(OH) (Fig. 3a) and the aniline $\delta_{oop}(NH_2)$ mode (Fig. 3b) follow the same trend, seeming to plateau at an aniline exposure of about 0.40 mmol $g_{(cat)}^{-1}$; the bonding here is attributed to adsorption at Pd/support interfacial sites. The 'knee' in the profile of the ν(OH) and $\delta_{oop}(NH_2)$ modes roughly coincides with the emergence of CHA $\nu_{AS}(CH_2)$ (Fig. 3c) and $\nu_S(CH_2)$ (Fig. 3d) bands. This inverse relationship is indicative of aniline adsorbed in a parallel orientation at the Pd(100)/support interface undergoing hydrogenation to CHA upon saturation. Thus, hydrogenation occurs upon saturation of the interfacial species.

For exposures $>1.13_{(ANL)} + 28.4_{(H_2)}$ mmol $g_{(cat)}^{-1}$, the ν(OH) (Fig. 3a) and the aniline $\delta_{oop}(NH_2)$ (Fig. 3b) modes diverge, with the ν(OH) mode showing continued augmentation, whilst the peak area for the aniline $\delta_{oop}(NH_2)$ mode is unchanged. As per Fig. 1, bands corresponding to in-plane modes of aniline, an indication of aniline adsorption to hydroxyl groups in isolation from the Pd crystallites, were first observable post-exposure of $1.13_{(ANL)} + 28.4_{(H_2)}$ mmol $g_{(cat)}^{-1}$. Therefore, the observed variance of trends associated with peak area of the ν(OH) and aniline $\delta_{oop}(NH_2)$ modes reflects continued adsorption of aniline to the hydroxyl groups of the alumina support, whilst adsorption of aniline at the Pd(100)/support interfacial sites saturates, reaching a steady state between aniline adsorption and hydrogenation to CHA.

3.2 Comparison of aniline adsorption to Pd/Al_2O_3 with and without hydrogen

Fig. 4 compares spectra collected after exposures of 0.54 and 1.62 $mmol_{(ANL)}$ $g_{(cat)}^{-1}$ with and without hydrogen and reveals notable differences at low coverage. At the low exposure (0.54 $mmol_{(ANL)}$ $g_{(cat)}^{-1}$), the presence of hydrogen produces stronger negative hydroxyl features, a broad region between 3650–3000 cm^{-1} encompassing $\nu_{AS}(NH_2)$ and $\nu_S(NH_2)$ modes, and a pronounced band at 1647 cm^{-1}, compared to adsorption without hydrogen. In contrast, the higher-exposure spectra (1.62 $mmol_{(ANL)}$ $g_{(cat)}^{-1}$)—where adsorption continues to increase—show broadly similar profiles, with the hydrogen-free spectrum (Fig. 4b) exhibiting a higher-intensity aniline band. These trends are thought to indicate that the differences in spectral profiles noted at the lower exposure arise from ANL hydrogenation to CHA.

The primary difference associated with adsorption with and without hydrogen is the formation of CHA. CHA, like aniline, contains NH_2 functionality, with $\nu_{AS}(NH_2)$ and $\nu_S(NH_2)$ at 3352 and 3274 cm^{-1}, respectively. In addition, CHA presents two in-plane NH_2 deformation modes ($\delta_{ip}(NH_2)$) associated with a shoulder feature at 3170 cm^{-1} and a medium intensity feature at 1617 cm^{-1}. Thus, the augmented broad feature at 1647 cm^{-1} and enhanced NH_2 stretching region seen in Fig. 4 are likely to reflect CHA adsorption alongside aniline.

Given prior evidence that CHA and aniline occupy different sites, it is intriguing to speculate on the bonding geometry of bound CHA. With reference to

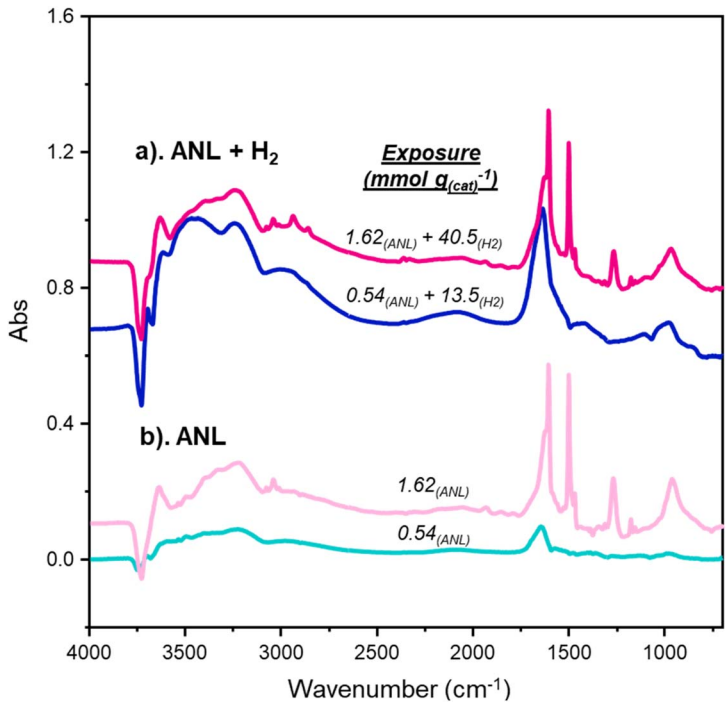

Fig. 4 DRIFTS spectra corresponding to 0.54 and 1.62 $mmol_{(ANL)}$ $g_{(cat)}^{-1}$ exposures to Pd/Al_2O_3 at 30 °C: (a) with a H_2 co-feed and (b) in the absence of a H_2 co-feed. The spectra have been offset to facilitate viewing. No additional manipulations were performed.

the metal-surface selection rule (MSSR),[21] the adsorption geometry of CHA on Pd(100) facets may also be hypothesized. Fig. 1 and 4 present a significant contribution from the $\delta_{ip}(NH_2)$ CHA modes compared to the usually high-intensity $\nu_{AS}(CH_2)$ and $\nu_S(CH_2)$ modes. In relation to dipole orientation, the $\nu_{AS}(CH_2)$ and $\nu_S(CH_2)$ modes possess dipoles that are out-of-plane with respect to the molecular axis at an angle < 90°. Contrarily, the $\delta_{ip}(NH_2)$ modes possess dipoles aligned directly with the molecular axis. Thus, during a vertical adsorption of CHA over a metal surface (Fig. 5), the $\delta_{ip}(NH_2)$ modes would experience significant augmentation from the perpendicular alignment of associated dipoles with the metal surface; whilst the out-of-plane $\nu_{AS}(CH_2)$ and $\nu_S(CH_2)$ modes would undergo slight, but not complete, shielding due to the out-of-plane elements of their associated dipole moments. Therefore, a suggested assignment of CHA adsorption geometry on Pd/Al_2O_3 is *via* vertical adsorption to the Pd(100) facets.

Moreover, both the in-plane $\delta_{ip}(NH_2)$ of CHA[18] and the out-of-plane $\delta_{oop}(NH_2)$ of aniline[16] are reported to occur at *ca.* 1620 cm^{-1}. Thus, emergence of the combination of these modes at 1647 cm^{-1} represents a noticeable shift (27 cm^{-1}). Therefore, binding is proposed to arise *via* the NH_2 functionality of CHA, as previously deduced with ANL.[16]

3.3 Temperature-programmed IR: aniline and H_2 desorption from Pd/Al_2O_3

TP-IR spectra following co-adsorption of aniline and hydrogen ($4.86_{(ANL)}$ + $122_{(H_2)}$ mmol $g_{(cat)}^{-1}$) on Pd/Al_2O_3 are shown in Fig. 6. Aniline bands decreased progressively with temperature, yet no orientational change was observed; key in-plane (ν(Ph–NH_2), $\mathcal{M}_{24}$ ν(CC), $\mathcal{M}_4$ ν(CC) at 1278, 1500, 1601 cm^{-1}) and out-of-plane ($\delta_{oop}(NH_2)$ at 1636 cm^{-1}) modes remained distinct throughout desorption. A negative hydroxyl feature near 3730 cm^{-1} persisted even after heating to 200 °C, indicating residual aniline bound to alumina hydroxyls.

Interestingly, the CHA bands initially intensified during heating. Peak area trends (Fig. 7) show an inverse relationship: ANL ν(Ph-NH_2) decreases while CHA $\nu_S(CH_2)$ increases between 30–120 °C, confirming hydrogenation of interfacial aniline within this temperature range to CHA. CHA formation ceases beyond 160 °C, marking 120–160 °C as the temperature range where aniline desorbs from Pd(100)/support sites.

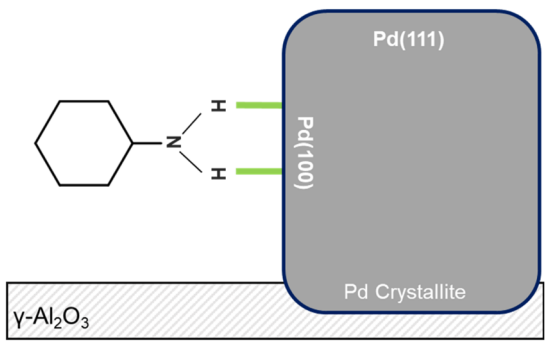

Fig. 5 Visualisation of vertical CHA bonding to Pd(100).

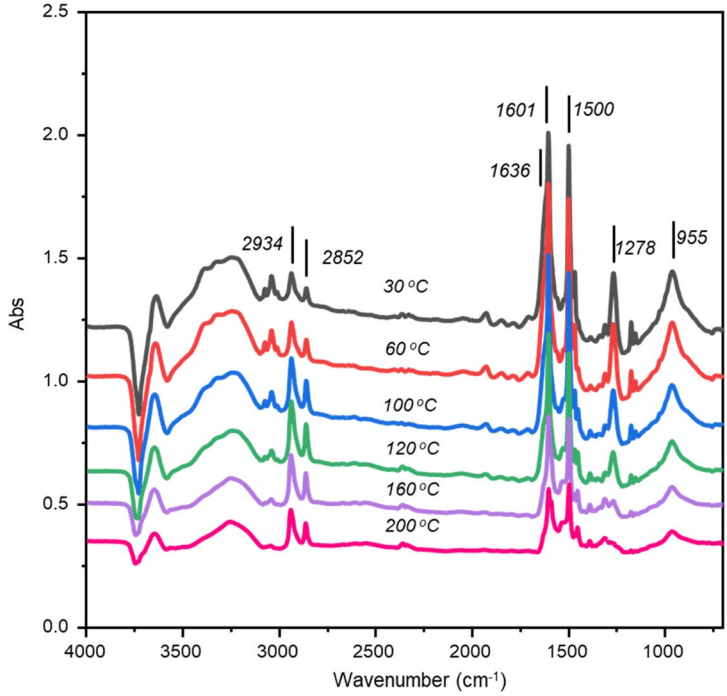

Fig. 6 TP-IR DRIFTS spectra (4000–700 cm^{-1}) of aniline and hydrogen adsorbed to Pd/Al_2O_3 as a function of increasing temperature: 30–200 °C. The spectra have been offset to facilitate viewing.

Fig. 6 shows some broadening at *ca.* 1640 cm^{-1} was observed for temperatures ≥160 °C. This is assigned to the shifted in-plane $\delta_{ip}(NH_2)$ mode of CHA that previously was associated with an element of CHA adsorption to the metal. The

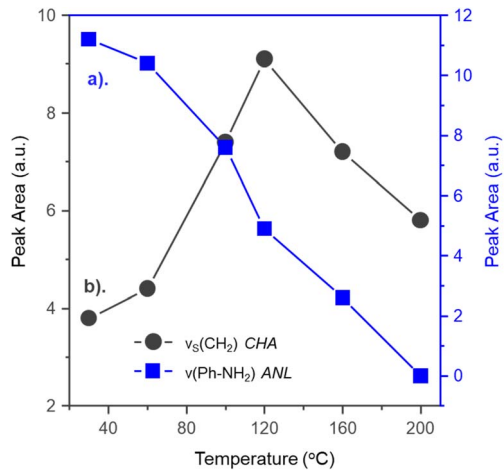

Fig. 7 Plot of peak area for bands corresponding to the (a) aniline ν(Ph-NH_2) and (b) cyclohexylamine $\nu_S(CH_2)$ modes as a function of increasing desorption temperature.

intensity of this feature compared to the $\nu_{AS}(CH_2)$ and $\nu_S(CH_2)$ modes (2936 and 2852 cm^{-1}) is far weaker than observed for low aniline and hydrogen exposures over the catalyst (Fig. 1). Therefore, the presence of the shifted $\delta_{ip}(NH_2)$ mode indicates some retention of CHA adsorption to the metal at this temperature, with the dominant CHA population residing on type IIa and type IIb hydroxyl groups of the alumina support.

After desorption at the maximum temperature, the medium intensity ν(Ph–NH_2) mode of aniline was no longer distinct; however, the high intensity $\mathcal{M}_{24}$ ν(CC) and $\mathcal{M}_4$ ν(CC) modes remained (Table S1). Thus, a limited population of aniline remained adsorbed to the OH groups of the alumina support after desorption at 200 °C, such that the medium intensity ν(Ph–NH_2) was not observed. A greater quantity of CHA remained.

From consideration of the hydroxyl region of Fig. 8, prior to temperature ramping (30 °C spectrum), two negative features were observed at 3728 and 3690 cm^{-1} that correspond to aniline/CHA H-bonding to type IIb and type III hydroxyls, respectively. Upon increasing the desorption temperature to 100 °C, the hydroxyl region is resolved such that the band corresponding to aniline/CHA H-bonding with type IIa hydroxyls at 3754 cm^{-1} was also distinct. Also, the feature aligned with H-bonding to type III hydroxyls was not observed; thus, aniline/CHA H-bonded to type III hydroxyls was desorbed in the temperature range of 60–100 °C.

In contrast to sole aniline adsorption TP-IR measurements,[16] the profiles associated with spectra from aniline and hydrogen adsorption to Pd/Al_2O_3 collected post-desorption at 160 and 200 °C clearly depict the type IIa OH site

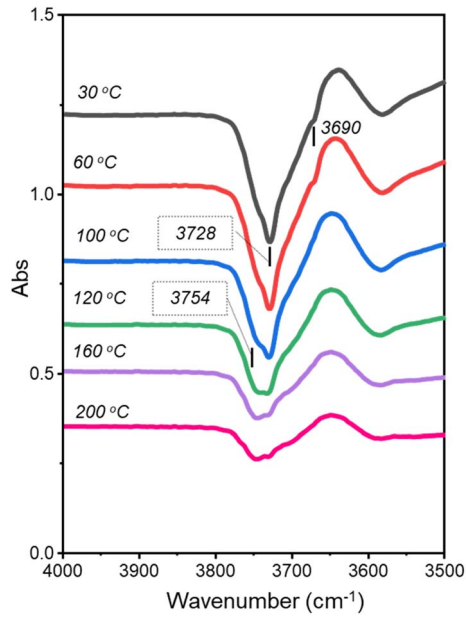

Fig. 8 DRIFTS spectra (4000–3500 cm^{-1}) depicting the hydroxyl group stretching region during increasing temperature (30–200 °C) post aniline and hydrogen co-adsorption to Pd/Al_2O_3. The spectra have been offset to facilitate viewing.

($3754\ cm^{-1}$) to be the dominant H-bonding adsorption site for this temperature range. This indicates stronger hydrogen-bonding of CHA with the hydroxyl support than aniline.

The updated binding strength hierarchy for ANL and CHA on Pd/Al_2O_3 is as follows: Type III OH (ANL/CHA) < Pd(100)/support interface (ANL) < Pd(100) (CHA) < Type IIb OH (ANL/CHA) < Type IIa OH (ANL/CHA).

4. Discussion

Historically, aniline over-hydrogenation to CHA, DICHA and CHAN has been the dominant route to lowered aniline selectivity during nitrobenzene hydrogenation,[2,6,8,9] with hydrogen loading identified as the dominant factor driving aniline hydrogenation over Pd/Al_2O_3.[16] Since this transformation represents the primary route to by-product formation, understanding its origin is essential for optimizing selectivity in nitrobenzene hydrogenation. Fig. 9 schematically illustrates the adsorption complexity underpinning these outcomes. Insights from this paper and collective works of the authors[8,15] presents the following framework:

(i) Nitrobenzene adsorbs on Pd(111) planes *via* monodentate binding in a vertical or slightly tilted orientation, limiting aromatic ring hydrogenation and suppressing nitrobenzene derived by-products.

(ii) In the presence of hydrogen, nitrobenzene predominantly converts to aniline.

(iii) Aniline can re-adsorb at Pd(100)/support interfacial sites in a parallel orientation, interacting through its nitrogen lone pair with Pd and forming H-bonds with adjacent alumina hydroxyls.

(iv) Aniline predominantly adsorbs on type IIa, IIb, and III hydroxyl groups of the alumina support. This preference for the inactive support restricts further

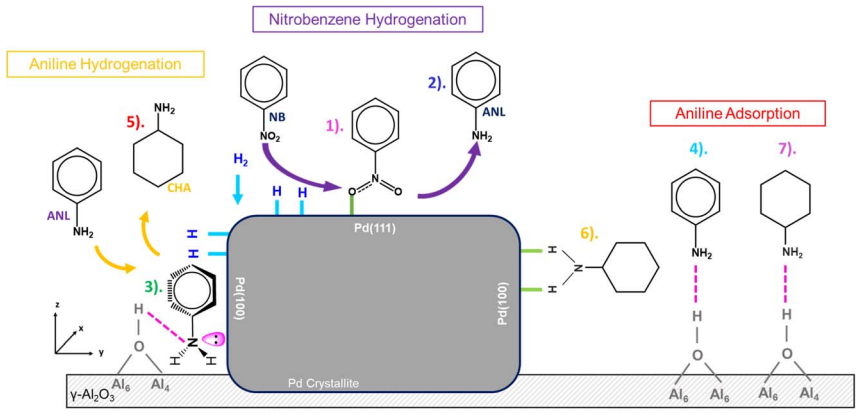

Fig. 9 Diagram visualising nitrobenzene (NB) adsorption to Pd(111) in a vertical orientation *via* one Pd–O bond, with subsequent hydrogenation to aniline (ANL), parallel aniline adsorption with respect to the metal at the support/Pd(100) interface, hydrogenation of parallel adsorbed aniline to cyclohexylamine, vertical bidentate CHA adsorption on Pd(100) and adsorption of aniline and CHA to the support with no specific geometry identified. The solid grey box represents a non-specific Pd crystallite; the hashed box represents the support. Larger arrows for vertical NB hydrogenation to ANL depicts this as the major transformation.

hydrogenation, explaining the inherent selectivity of Pd/Al_2O_3 catalysts for aniline synthesis.

(v) Aniline adsorbed in a parallel orientation at Pd(100)/support interfaces undergoes hydrogenation to CHA, enabled by the planar alignment of the aromatic ring with the active Pd surface.

(vi) CHA can re-adsorb vertically on Pd(100) *via* bidentate binding.

(vii) CHA also resides on type IIa, IIb, and III hydroxyl sites of the alumina support, where strong H-bonding prevents further transformation to *N*-cyclohexylcyclohexylaniline (CHAN).

Collectively, these observations reveal a sequence of adsorption and transformation steps that govern selectivity: nitrobenzene activation on Pd(111), aniline formation and interfacial hydrogenation on Pd(100), and eventual stabilization of CHA on alumina hydroxyls. This interplay between metal and support sites explains why Pd/Al_2O_3 catalysts favour aniline synthesis and limit deeper hydrogenation. The mechanistic picture presented here provides a foundation for rational catalyst design and indicates the suitability of Pd/Al_2O_3 as a candidate aniline synthesis catalyst.

5. Conclusions

Infrared spectroscopy combined with application of the MSSR enabled the derivation of a detailed structure–activity relationship governing selective aniline synthesis over Pd/Al_2O_3 catalysts. This approach demonstrates how catalytic selectivity can be rationalized from fundamental IR principles. The key conclusions are as follows:

• Hydroxyl site interactions: strong negative OH features at 3754, 3728, and 3690 cm^{-1} confirm adsorption of aniline and CHA on type IIa, IIb, and III hydroxyl groups of the γ-Al_2O_3 support.

• Low-coverage adsorption geometry: At $\leq 0.54_{(ANL)} + 13.5_{(H_2)}$ mmol $g_{(cat)}^{-1}$, spectra show only out-of-plane aniline modes and negative OH features, consistent with parallel adsorption at Pd/support interfacial sites.

• CHA formation: bands at 2934 and 2852 cm^{-1}, assigned to $\nu_{AS}(CH_2)$ and $\nu_S(CH_2)$, appear at exposures $\geq 1.08_{(ANL)} + 27.0_{(H_2)}$ mmol $g_{(cat)}^{-1}$, indicating hydrogenation of adsorbed aniline to CHA.

• Combined NH_2 deformation features: enlargement of the broad band near 1650 cm^{-1} under the hydrogen co-feed reflects overlapping $\delta_{oop}(NH_2)$ (aniline) and $\delta_{ip}(NH_2)$ (CHA) modes, indicative of NH_2-mediated binding to Pd surfaces.

• CHA orientation: enhanced $\delta_{ip}(NH_2)$ intensity relative to out-of-plane CH_2 stretches at low coverage indicates vertical CHA adsorption on Pd(100).

• High-coverage behaviour: at exposures of $\geq 1.13_{(ANL)} + 28.4_{(H_2)}$ mmol $g_{(cat)}^{-1}$, all aniline modes appear alongside intensified OH features, confirming adsorption shifts to alumina hydroxyls. CHA modes dominate, indicating CHA stabilization on the support.

• Site differentiation: peak-area trends and TP-IR confirm CHA occupies additional sites beyond those of aniline, including Pd(100) planes, where CHA adsorbs vertically.

• Binding hierarchy: TP-IR establishes the order of adsorption strength: Type III OH (ANL/CHA) < Pd(100)/support interface (ANL) < Pd(100) (CHA) < Type IIb OH (ANL/CHA) < Type IIa OH (ANL/CHA).

Overall, these findings reveal that hydrogen loading drives CHA formation *via* interfacial aniline hydrogenation, while strong aniline adsorption on alumina hydroxyls limits deeper hydrogenation. This mechanistic understanding provides a basis for rational catalyst design.

Author's contribution

Annelouise McCullagh: methodology, formal analysis, investigation, data curation, writing – original draft, writing – review & editing; David Lennon: conceptualization, methodology, resources, writing – review & editing, supervision, project administration, funding acquisition.

Conflicts of interest

There are no conflicts of interest.

Data availability

Datasets for the article are available from the University of Glasgow Library.

Supplementary information (SI): Table 1: comparison of experimental and DFT-derived wavenumbers of aniline; Fig. S1: plot of peak area for bands corresponding to (a) aniline ν(Ph-NH_2), (b) cyclohexylamine $\nu_S(CH_2)$, and (c) $\nu_{AS}(CH_2)$ modes as a function of increasing aniline and H_2 exposure. See DOI: https://doi.org/10.1039/d5fd00169b.

Acknowledgements

The EPSRC are thanked for the provision of a PhD studentship (ALMcC, EP/R513222/1 & EP/N509668/1).

References

1 T. Kahl, K. W. Schröder, F. Lawrence, W. Marshall, H. Höke and J. R. Aniline, in *Ullmann's Encylopedia of Industrial Chemistry*, Wiley, Weinheim, 2012, pp 45–478.

2 C. S. Couto, L. M. Madeira, C. P. Nunes and P. Araújo, Hydrogenation of Nitrobenzene over a Pd/Al2O3 Catalyst – Mechanism and Effect of the Main Operating Conditions, *Chem. Eng. Technol.*, 2015, **38**(9), 1625–1636, DOI: 10.1002/ceat.201400468.

3 E. A. Gelder, S. D. Jackson and C. M. Lok, The Hydrogenation of Nitrobenzene to Aniline: A New Mechanism, *Chem. Commun.*, 2005, (4), 522–524, DOI: 10.1039/B411603H.

4 S. Kataoka, Y. Takeuchi, A. Harada, T. Takagi, Y. Takenaka, N. Fukaya, H. Yasuda, T. Ohmori and A. Endo, Microreactor Containing Platinum Nanoparticles for Nitrobenzene Hydrogenation, *Appl. Catal. Gen.*, 2012, **427–428**, 119–124, DOI: 10.1016/j.apcata.2012.03.041.

5 H. Jiang, G. Yuan, Z. Cui, Z. Zhao, Z. Dong, J. Zhang, Y. Cong and X. Li, Effects of Support Types and Their Porosity Characteristics on the Catalytic Performance of Ni-Based Catalysts in Nitrobenzene Hydrogenation to

Aniline, *Ind. Eng. Chem. Res.*, 2023, **62**(34), 13355–13367, DOI: 10.1021/acs.iecr.3c01327.

6 C. G. A. Morisse, A. M. McCullagh, J. W. Campbell, C. Mitchell, R. H. Carr and D. Lennon, Mechanistic Insight Into the Application of Alumina-Supported Pd Catalysts for the Hydrogenation of Nitrobenzene to Aniline, *Ind. Eng. Chem. Res.*, 2022, **61**(30), 10712–10722, DOI: 10.1021/acs.iecr.2c01134.

7 G. Brereton, Polyurethanes, in *Ullmann's Encyclopedia of Industrial Chemistry*, Wiley, Weinheim, 2019, pp. 1–76.

8 J. W. Campbell, A. M. McCullagh, L. McGrath, C. How, D. A. MacLaren, M. Loenders, N. Meyer, R. H. Carr and D. Lennon, The Application of Alumina Supported Pd Catalysts for High Selectivity Aniline Synthesis Catalysis at Elevated Temperatures: Site-Selective Chemistry, *Appl. Catal. Gen.*, 2024, **670**, 119541, DOI: 10.1016/j.apcata.2023.119541.

9 C. G. A. Morisse, A. M. McCullagh, J. W. Campbell, C. How, D. A. MacLaren, R. H. Carr, C. J. Mitchell and D. Lennon, Toward High Selectivity Aniline Synthesis Catalysis at Elevated Temperatures, *Ind. Eng. Chem. Res.*, 2021, **60**(49), 17917–17927, DOI: 10.1021/acs.iecr.1c03695.

10 T. J. Rockey, M. Yang and H.-L. Dai, Aniline on Ag(1 1 1): Adsorption Configuration, Adsorbate–Substrate Bond, and Inter-Adsorbate Interactions, *Surf. Sci.*, 2005, **589**(1), 42–51, DOI: 10.1016/j.susc.2005.05.048.

11 S. X. Huang, D. A. Fischer and J. L. Gland, Correlation between the Surface Configurations and Hydrogenolysis: Aniline on the Pt(111) Surface, *J. Vac. Sci. Technol., A*, 1994, **12**(4), 2164–2169, DOI: 10.1116/1.579107.

12 Z. H. A. Alsunaidi, T. R. Cundari and A. K. Wilson, Toward a More Rational Design of the Direct Synthesis of Aniline: A Density Functional Theory Study, *ACS Omega*, 2017, **2**(7), 3214–3227, DOI: 10.1021/acsomega.7b00356.

13 I. Tezsevin, J. F. W. Maas, M. J. M. Merkx, R. Lengers, W. M. M. Kessels, T. E. Sandoval and A. J. M. Mackus, Computational Investigation of Precursor Blocking during Area-Selective Atomic Layer Deposition Using Aniline as a Small-Molecule Inhibitor, *Langmuir*, 2023, **39**, 4265–4273.

14 J. H. Henríquez-Román, L. Padilla-Campos, M. A. Páez, J. H. Zagal, M. A. Rubio, C. M. Rangel, J. Costamagna and G. Cárdenas-Jirón, The Influence of Aniline and Its Derivatives on the Corrosion Behaviour of Copper in Acid Solution: A Theoretical Approach, *J. Mol. Struct.:THEOCHEM*, 2005, **757**(1), 1–7, DOI: 10.1016/j.theochem.2005.05.018.

15 A. M. McCullagh, E. K. Gibson, S. F. Parker, K. Refson and D. Lennon, The Adsorption of Nitrobenzene over an Alumina-Supported Palladium Catalyst: An Infrared Spectroscopic Study, *Phys. Chem. Chem. Phys.*, 2023, **25**(38), 25993–26005, DOI: 10.1039/D3CP03028H.

16 A. M. McCullagh, S. F. Parker and D. Lennon, The Adsorption of Aniline over Alumina-Supported Palladium: An Infrared Spectroscopic and Computational Study, *Philos. Trans. R. Soc., A*, 2026, **384**, 20240556, DOI: 10.1098/rsta.2024.0556.

17 A. M. McCullagh and D. Lennon, *The Hydrogenation of Aniline over an Alumina-Supported Pd Catalyst*, Submitted for publication, 2025.

18 J.-Y. T. Chen and J. H. Gould, Infrared Studies of Cyclohexylamine, *J. Assoc. Off. Anal. Chem.*, 1972, **55**(5), 1006–1014, DOI: 10.1093/jaoac/55.5.1006.

19 I. D. Darkhalil, J. J. Klaassen, B. S. Deodhar, T. K. Gounev and J. R. Durig, Conformational Stability, Infrared and Raman Spectra, Vibrational

Assignments, and Theoretical Calculations of Cyclohexylamine, *J. Mol. Struct.*, 2015, **1088**, 169–178, DOI: 10.1016/j.molstruc.2015.02.007.

20 H. Knozinger and P. Ratnasamy, Catalytic Aluminas: Surface Models and Characterisation of Surface Sites, *J. Eng. Sci.*, 1978, **17**, 31–70, DOI: 10.1080/03602457808080878.

21 R. G. Greenler, D. R. Snider, D. Witt and R. S. Sorbello, The Metal-Surface Selection Rule for Infrared Spectra of Molecules Adsorbed on Small Metal Particles, *Surf. Sci.*, 1982, **118**(3), 415–428, DOI: 10.1016/0039-6028(82)90197-2.